Synthesis of Bi_2WO_6 Nanometer Sheet Shaped and Approach to the Photocatalysis

Dong Young Kim, Sujung Kim, and Misook Kang*

Department of Chemistry, College of Science, Yeungnam University, Gyeongsan, Gyeongbuk 712-749, Korea
**E-mail: mskang@ynu.ac.kr*
Received November 28, 2008, Accepted January 19, 2009

For use as a photocatalyst, bismuth tungsten oxide, Bi_2WO_6, was successfully synthesized by hydrothermal treatment at pH = 11 and heating at 200 °C for 24 h, and samples were subsequently thermal treated at 400, 600, and 800 °C to increase crystallinity. TEM results revealed that the initial untreated particles were sheet-shaped, grain size was below 80 nm, and it increased with treated temperatures. These Bi_2WO_6 samples absorbed at around 400 nm in the visible light range and the intensity of absorption was particularly strongest in samples thermal treated at 600 °C. Their photoluminescence abilities, related to the recombination between the excited electrons and holes, were overall small for other general photocatalysts such as TiO_2, and the smallest in the case of thermal treatment at 600 °C, as reversible result of UV-visible absorbance. Methyl orange of 5.0 ppm aqueous solution was almost completely removed after 2 h when treated over the Bi_2WO_6 thermal treated at 600 °C.

Key Words: Bi_2WO_6, Thermal treatment, Photoluminescence, Methyl orange removal

Introduction

Semiconductor photocatalysts have attracted great interest for their potential applications in environmental treatments, hydrogen evolution from the hydrolysis of water, the fixation of CO_2 and N_2, and the photosynthesis of organic compounds.[1-3] TiO_2 is by far the most popular photocatalyst, desired for its high activity, good photostability, non-toxicity, and low price. But the large band gap of TiO_2 (3.2 eV) makes it excitable only by UV light wavelengths below 387 nm, which severely limits the efficient usage of solar energy to a maximum of 5% and hinders the commercialization of this technology.[4-10] Therefore, to avoid this drawback, new visible-light-driven photocatalysts have been explored. Recently, nano-structured tungsten materials, such as Bi_2WO_6, Bi_2MO_6, $Bi_2W_{1-x}Cu_xO_{6-2x}$, and Sb_2WO_6, have attracted much interest because of their potential application in various fields, including photoluminescence, optical fiber, scintillation materials, and photocatalysts.[11-14] These materials have unique combinations of physical and chemical properties, such as electronic versatility, reactivity, and stability.

Bi_2WO_6 has been reported to be particularly photocatalytically active for the breakdown of dye compounds (Fu *et al.*[15]); RhB at 10 ppm photodestructed in 240 minutes over 0.5 grams of Bi_2WO_6 prepared at 180 °C. It is wellknown that Bi_2WO_6 exhibits higher activity than TiO_2 and has potential uses in environmental remediation induced by solar energy.[16,17] Unfortunately Bi_2WO_6 has a higher molecular weight than TiO_2 and is more difficult to disperse in aqueous solution, a serious drawback for heterogeneous photocatalysis. In addition, when particle size is decreased, the decreased crystallinity resulted in lower photocatalytic activity. Therefore, in this study, we tried to control the particle size of Bi_2WO_6 nanosheet to below 100 nm using a hydrothermal treatment at high temperature (200 °C) and pressure (20 atm). Crystallinity was then increased by thermal treatment at temperatures above 400 °C. The resulting Bi_2WO_6 nanosheet photocatalysts were then assesed for their photocatalytic activity in the removal of methyl orange from solution.

Experimental Section

Preparation of Bi_2WO_6 photocatalysts. The Bi_2WO_6 nanometer-sized sheet-shaped particles were prepared using a commercial hydrothermal method as shown in Figure 1. Bi^{3+} ($Bi(NO_3)_3 \cdot 5H_2O$, 99.9%) and W^{6+} ion precursors (WCl_6, 99.9%) were mixed with distilled water, with the mole ratio of Bi^{3+}:W^{6+} kept at 1.0:2.0 and the pH of the solution maintained at 9.0 with ammonium hydroxide. After 5 h of stirring to obtain a homogeneous state, the final solution was transferred to an autoclave, which was then heated to 200 °C at a rate of 5 °C/min and held at this temperature for 24 h. The autoclave was maintained with nitrogen gas at 20.0 atm to produce smaller crystallite size. During the thermal treatment, bismuth and tungsten were hydrolyzed by the OH group in the water and crystallites of Bi_2WO_6 with an orthorhombic structure then appeared. The powders obtained were washed in distilled water and dried at 100 °C for 24 h. Finally, these were thermal treated at 400, 600, and 800 °C for 3 h to get the higher crystallinity.

Characteristics of Bi_2WO_6 photocatalysts. The synthesized Bi_2WO_6 powders were subjected to X-ray diffractometry (XRD, Yeungnam University Instrumental Analysis Center, Korea; Model PW 1830, Philips, Amsterdam, The Netherlands) with nickel-filtered Cu$K\alpha$ radiation (30 kV, 30mA) from 5° to 70°, with a scan speed of 10° min^{-1} and time constant of 1 s. The sizes and shapes of the Bi_2WO_6 particles were determined using scanning electron microscopy (SEM, Yeungnam University Instrumental Analysis Center, Korea; Model JEOL-JSM35CF, Tokyo, Japan). High-resolution transmission electron microscopy (TEM, Yeungnam University Instrumental Analysis Center, Korea) images of the nanometer-

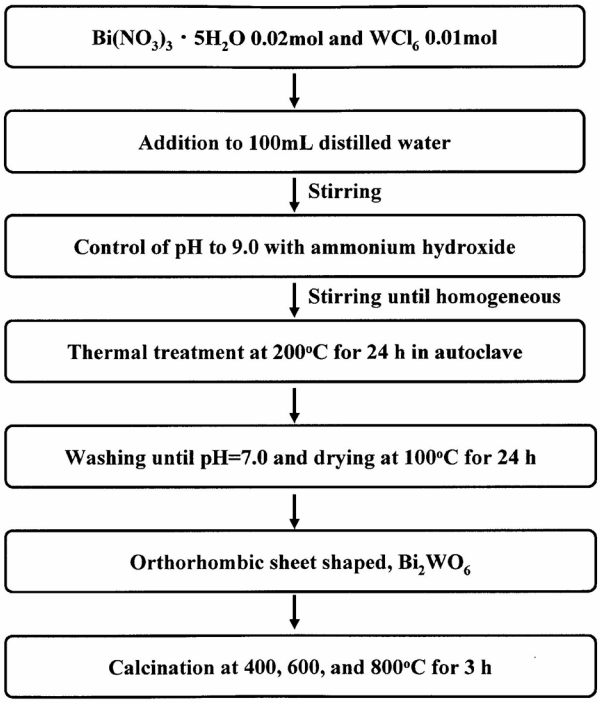

Figure 1. The preparation of Bi_2WO_6 nanosheet particles using a commercial hydrothermal method.

sized samples were obtained on a JEOL 2000EX transmission electron microscope operated at 200 kV. The UV-visible spectra of the Bi_2WO_6 powders were obtained using a Shimadzu MPS-2000 spectrometer (Kyoto, Japan) with a reflectance sphere over the special range of 200 to 800 nm.

Photoluminescence (PL, Research Institute of Basic Sciences Sunchon National University, Korea) spectroscopy measurements of the Bi_2WO_6 powders were also conducted to examine the number of photo-excited electron hole pairs in each of the samples. Samples as 1.0 mm pellets were measured at room temperature using a He-Cd laser source at a wavelength of 325 nm. X-ray photon spectroscopy (XPS, Cooperative Center to Research Facilities, Sungkyunkwan University Instrumental Analysis Center, Korea) measurements of Bi4f, W4f, and O1s were recorded with an ESCA 2000 (VZ MicroTech, Oxford, UK) system, equipped with a non-monochromatic Al*K*α (1486.6 eV) X-ray source. The Bi_2WO_6 powders were pelletized, at 1.2×10^4 kPa for 1 min, and the 1.0-mm pellets were then maintained overnight in a vacuum (1.0×10^{-7} Pa) to remove water molecules from the surface prior to measurement. The base pressure of the ESCA system was below 1×10^{-9} Pa. Experiments were recorded with a 200 W power source and an angular acceptance of ± 5º. The analyzer axis made an angle of 90º with the specimen surface. Wide scan spectra were measured over a binding energy range of 0 to 1200 eV, with pass energy of 100.0 eV. The Ar^+ bombardment of the Bi_2WO_6 was performed with an ion current of 70 to 100 nA over an area of 10.0 × 10.0 mm with a total sputter time of 2400 s divided into 60 s intervals. A Shirley function was used to subtract the background in the XPS data analysis. The O1s, Bi4f, and W4f XPS signals were fitted using mixed Lorentzian-Gaussian curves.

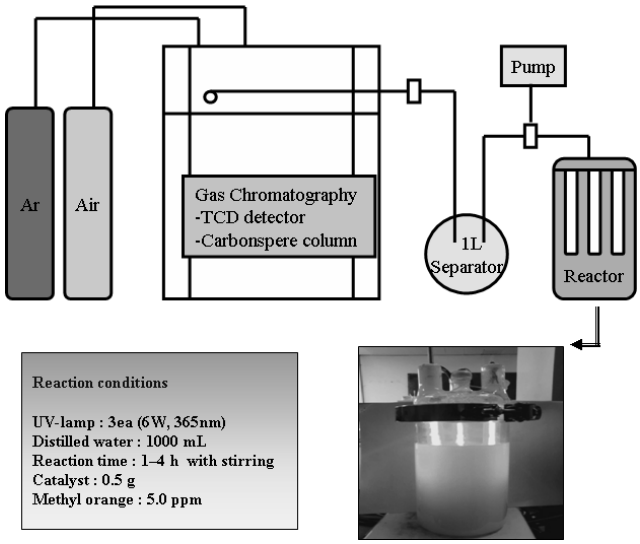

Figure 2. The photoreactor for methyl orange removal (decomposition).

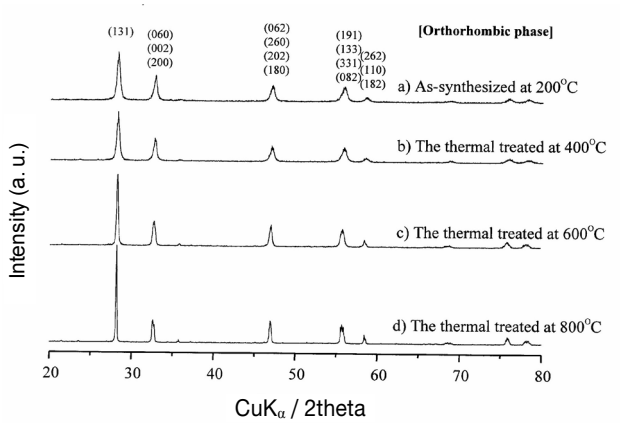

Figure 3. The XRD patterns of the Bi_2WO_6 particles thermal treated at various temperatures.

Photodecomposition of methyl orange. The decomposition of methyl orange was carried out using bed photo reactors designed in the laboratory (Figure 2). In preparation for the methyl orange decomposition, Bi_2WO_6s powder of 0.5 g/1000 mL solution were added into a pyrex cylinder reactor with 2.0 L volume. The initial concentration of methyl orange was 5.00 ppm. A UV-lamp (model BBL, 24 W/cm^2, 30 cm length × 2.0 cm diameter, Shinan Co., Korea) emitting 365 nm light was used. The methyl orange decomposition was performed in the condition without air bubbling. Analyses of the concentration of methyl orange in the reaction solution before and after the reaction were done using UV-visible spectroscopy.

Results and Discussion

Figure 3 shows the XRD patterns of the Bi_2WO_6 particles thermal treated at various temperatures. The Bi_2WO_6 particles, all the samples exhibited an orthorhombic structure. The orthorhombic structure had peaks at 28.3, 32.7, 47.1,

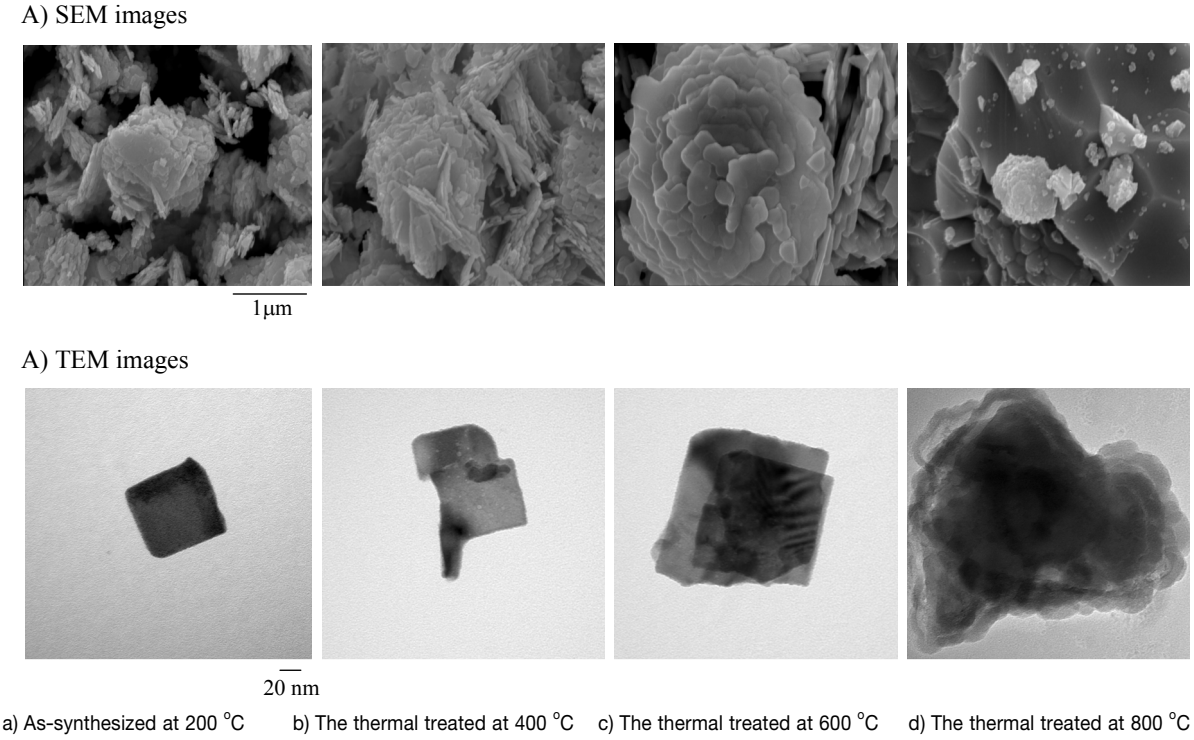

Figure 4. The SEM and TEM photographs of thermal treated Bi_2WO_6 at various temperatures.

55.7, and 58.5, which are assigned to the (d_{131}), ($d_{200, 060}$), ($d_{180, 202, 260}$), ($d_{082, 133, 191}$), and ($d_{182, 110, 262}$) planes, respectively.[18,19] The peak intensities increased with the increase of the treated temperature, however, no other peaks assigned to Bi_2O_3 or WO_3, which would indicate their presence on the external surface of the Bi_2WO_6 framework, were seen in the XRD patterns of any of the samples. On the other hand, the line widths of the peaks were broad; generally, the larger the line-broadening of the peaks, the smaller the crystalline domain sizes. Scherrer's equation, $\tau = 0.9\lambda/\beta\cos\theta$, where λ is the wavelength of the incident X-rays, β is the full width at half maximum height in radians, and θ is the diffraction angle, was used to determine the crystalline domain size. The calculated crystalline domain sizes in the plane (131) were 17, 25, 24, and 23 nm for the as-synthesized (not thermal treated) product, the thermal treated at 400 °C, 600 °C, and 800 °C products, respectively.

Figure 4 shows the SEM and TEM photographs of the particle shapes of thermal treated Bi_2WO_6. A relatively uniform mixture of nanosheet shaped particles whose sizes were distributed in the 80-100 nm range, was shown in these photographs. Their size was increased in the samples prepared at higher temperatures, owing to the agglomeration induced by a considerable sintering effect. This corresponds to the results of the XRD analysis shown in Figure 3.

Table 1 summarizes the physical properties of the thermal treated Bi_2WO_6 powders. From the energy dispersive analysis of X-rays (EDAX), the true atomic ratios of bismuth/tungsten in the as-synthesized product, and the thermal treated at 400, 600, and 800 °C products were found to be 2.03, 2.31, 2.51, and 2.41, respectively, indicating the separation of the tungsten ion from Bi_2WO_6 orthorhombic framework at higher

Table 1. The physical properties of the thermal treated Bi_2WO_6 powders.

Elements / Catalysts	Atomic compositions Bi	W	O	Bi/W	O/Bi+W
As-synthesized	55.82	27.53	16.65	2.03	0.20
The thermal treated at 400 °C	58.16	25.07	16.77	2.31	0.20
The thermal treated at 600 °C	61.53	24.43	14.04	2.51	0.16
The thermal treated at 800 °C	58.11	24.11	17.70	2.41	0.22

temperatures, with the largest effect in the Bi_2WO_6 thermal treated at 600 °C. Additionally, the atomic ratio of O/(B+W) is also the smallest in the sample, indicating the framework anion defect which related to conduction properties. The framework defect leads to easier electron transfer to the conduction band, and suppressed the recombination of electrons and holes during photocatalysis.

Quantitative XPS analyses of the Bi_2WO_6 particles were performed, with the typical survey and high-resolution spectra shown in Figure 5. The $Bi4f_{5/2}$ and $Bi4f_{7/2}$ spin-orbital splitting photoelectrons for anatase Bi_2O_3 were located at binding energies of 164.4 and 159.1 eV, respectively, and assigned to the presence of typical Bi^{3+} in the as-synthesized product.[20] When it was treated at 600 °C, the bands were a little broader, and shifted slightly to a higher binding energy of 164.60 and 159.3 eV for $Bi4f_{5/2}$ and $Bi4f_{7/2}$, respectively, which might be assigned to more oxidized Bi ions. The differences (delta) in binding energies between $Bi4f_{5/2}$ and $Bi4f_{7/2}$ were distributed in the range of 5.25~5.40 eV in all of the Bi_2WO_6 particles. The O1s region was decomposed into two contributions:

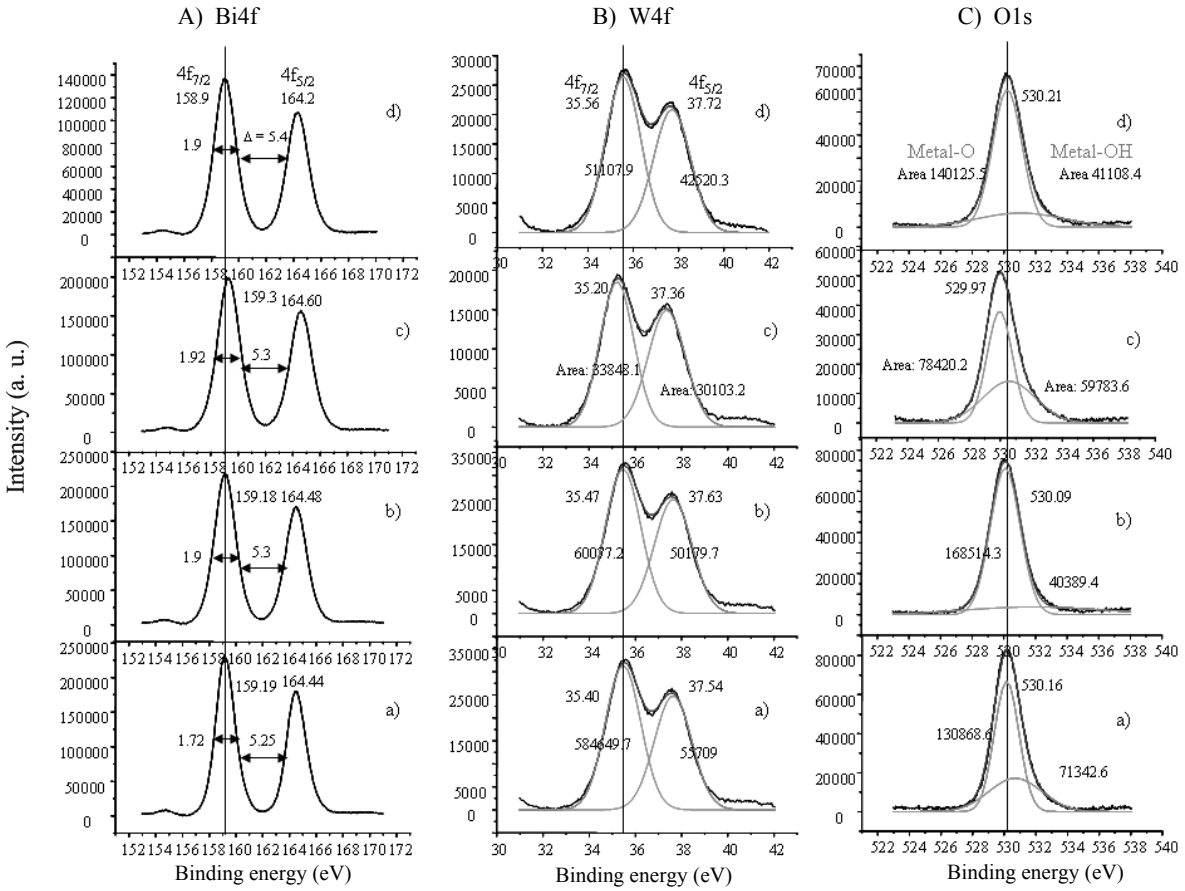

Figure 5. The XPS curves of thermal treated Bi_2WO_6 at various temperatures. a) As-synthesized, b) Thermal treated at 400 °C, c) Thermal treated at 600 °C, and d) Thermal treated at 800 °C

metal-O (530.2 eV) in the metal oxide and metal-OH (531.0 eV). The area ratio of metal-OH/metal-O in the O1s peaks were distinguishably increased in the sample thermal treated at 600 °C compared to those in other products, increasing in the magnitude of the ratio in the treated samples at 400 °C (0.240) < 800 °C (0.293) < 200 °C (as-synthesized, 0.545) < 600 °C (0.762). In general, a higher metal-OH peak indicated that the particles were more hydrophilic, and thus produced many more OH radicals during photocatalysis; consequently, its photocatalytic activity could be improved. The $W4f_{7/2}$ and $W4f_{5/2}$ spin-orbital splitting photoelectrons for WO_3 were located at binding energies of 35.40 and 37.54eV, respectively. When it was treated at 600 °C, the bands shifted slightly to a lower binding energy of 35.20 and 37.36eV for $W4f_{7/2}$ and $W4f_{5/2}$, respectively, which might be assigned to less oxidized W ions.

Figure 6 shows the UV-visible spectra of the Bi_2WO_6 powders thermal treated at various temperatures. The absorption normally appears first at around 400 nm in the samples prepared from all products. Generally, the band gaps in a semiconductor material are closely related to the wavelength range absorbed. The longer the absorption wavelength has, the shorter the band gap. Herein, it is postulated that the Bi_2WO_6 samples treated at higher temperatures have a shorter band gap than that of the non-treated sample, and that the band gap decreased in the order of the as-synthesized product = the product thermal treated at 400 °C > the product thermal treated at 600 °C > the product thermal treated at 800 °C.

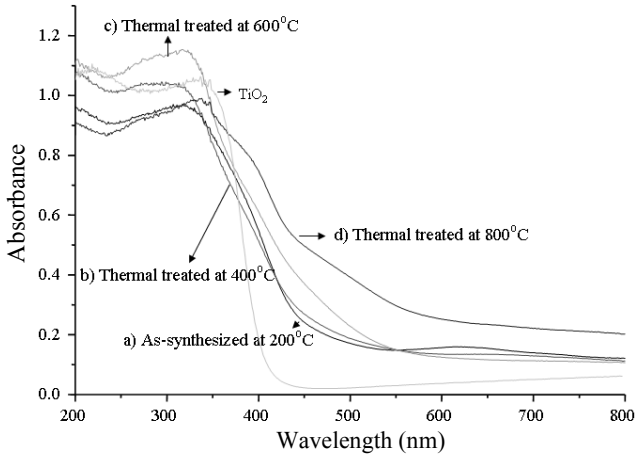

Figure 6. The UV-visible spectra of the Bi_2WO_6 powders thermal treated at various temperatures.

However, the absorption ability was the greatest in the Bi_2WO_6 thermal treated at 600 °C. The commercialized photocatalyst, TiO_2 with anatase structure, absorbs around 370 nm, which has been also expressed in this figure as a reference.

Figure 7 presents the photoluminescence (PL) spectra of Bi_2WO_6 powders thermal treated at various temperatures. The PL curve indicates that the electrons in the valence band transferred to the conduction band, and then the excited electrons were stabilized by photoemission. In general, if the

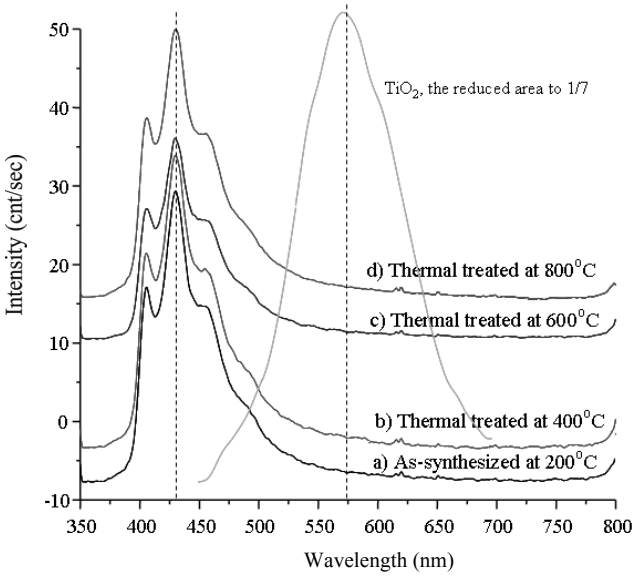

Figure 7. The photoluminescence (PL) spectra of Bi_2WO_6 powders thermal treated at various temperatures.

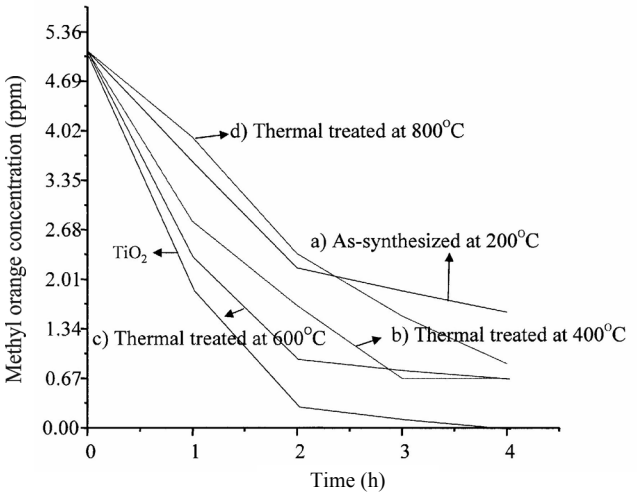

Figure 8. The methyl orange removal over thermal treated Bi_2WO_6 powders.

number of the emitted photons resulting from the recombination between excited electrons and holes is increased, the PL intensity increases, and consequently, the photo activity decrease. Therefore, there is a strong relationship between PL intensity and photo activity. In particular, when metal captures excited electrons the PL intensity decreases to an even greater extent. In this figure, the PL curves of Bi_2WO_6 powders were similar to that of general titania (TiO_2) photocatalysts with an emission at 450-650 nm. But their photoluminescence were overall very small compared with general titania photocatalysts. The PL curve is smallest in the case of thermal treatment at 600 °C, most likely due to the oxygen atoms playing the role of electron capturers as the expected result in Table 1, thereby depressing the recombination process. This result was reversible in UV-visible absorbance. Consequently, the PL intensity depends on whether the added tungsten metal was acted as an electron capturer or not.

Figure 8 gives the methyl orange decomposition over thermal treated Bi_2WO_6 powders. The decomposition rate was faster in the Bi_2WO_6 thermal treated at 600 °C, as might be expected by the physical properties explained in Table 1, Figure 5, and Figure 6.; methyl orange of 5.0 ppm mostly decomposed after 2 h. However, when the treated temperature was increased to 800 °C, the photodestruction of methyl orange decreased. This was in spite of having the lower band gap caused by considerable agglomeration between particles through sintering at higher temperatures, as shown in SEM and TEM images, and the increased recombination between electrons and holes suggested from the result of PL curves. Based on this observation, it was concluded that the optimum temperature treatment for Bi_2WO_6 photocatalyst was 600 °C to produce effective methyl orange decomposition and that this resulted from having a proper sized band gap and depressing the recombination between electrons and holes. This result confirmed that Bi_2WO_6 can be very useful as a photocatalyst for removal of dye compounds like methyl orange.

Conclusions

The following conclusions can be drawn from this study: the removal of methyl orange of 5.0 ppm was completely photodestructed after 2 h over the Bi_2WO_6 powder thermal treated at 600 °C, but effectiveness was rather decreased over Bi_2WO_6 powder thermal treated at 800 °C in spite of it having the lower band gap. Consequently, we found herein that the lower band gap did not always affect the photocatalytic activity, and depressing the recombination between electrons and holes was rather important. Additionally, when the Bi_2WO_6 is more and less oxidized, Bi and W ions are present and its photocatalytic performance is enhanced.

Acknowledgments. This work was supported by the National Center for Nanomaterials Technology through Yeungnam University in 2008.

References

1. Hoffmann, M. R.; Martin, S. T.; Choi, W.; Bahnemannt, D. W. *Chem. Rev.* 1**995**, *95*, 69.
2. Linsebigler, A. L.; Lu, G.; Yates Jr. J. T. *Chem. Rev*. **1995**, *95*, 735.
3. Carp, O.; Huisman, C. L.; Reller, A. *Progr. Solid State Chem*. **2004**, *32*, 33.
4. Almquist, C. B.; Biswas, P. *J. Catal*. **2002**, *212*, 145.
5. Sökmen, M.; Özkan, A. *J. Photochem. & Photobiol. A: Chem*. **2002**, *147*, 77.
6. Gelover, S.; Mondragón, P.; Jiménez, A. *J. Photochem. & Photobiol. A: Chem*. **2004**, *165*, 241.
7. Pore, V.; Heikkilä, M.; Ritala, M.; Leskelä, M.; Areva, S. *J. Photochem. & Photobiol. A: Chem*. **2006**, *177*, 68.
8. Tristão, J. C.; Magalhães, F.; Corio, P.; Terezinha, M.; Sansiviero, C. *J. Photochem. & Photobiol. A: Chem*. **2006**, *181*, 152.
9. Graf, C.; Ohser-Wiedemann, R.; Kreisel, G. *J. Photochem. & Photobiol. A: Chem*. **2007**, *188*, 226.
10. Ullah, R.; Dutta, J. *J. Hazard. Mater*. **2008**, *156*, 194.
11. Frit, B.; Mercurio, J. P. *J. Alloy. Compd*. **1992**, *188*, 27.
12. Sharma, V.; Shukla, A. K.; Gopalakrishnan, J. *J. Mater. Chem*. **1994**, *4*, 703.

13. Zhang, S.; Shen, J.; Fu, H.; Dong, W.; Zheng, Z.; Shi, L. *J. Solid State Chem*. **2007**, *180*, 1456.
14. Zhao, X.; Xu, T.; Yao, W.; Zhang, C.; Zhu, Y. *Appl. Catal. B: Environ*. **2007**, *72*, 92.
15. Fu, H.; Zhang, L.; Yao, W.; Zhu, Y. *Appl. Catal. B: Environ*. **2006**, *66*, 100.
16. Zhang, C.; Zhu, Y. F. *Chem. Mater*. **2005**, *17*, 3537.
17. Fu, H. B.; Pan, C. S.; Yao, W. Q.; Zhu, Y. F. *J. Phys. Chem. B: Environ*. **2005**, *109*, 22432.
18. Hsieh, C. Y.; Fung, K.-Z. *J. Phys. Chem. Solids* **2008**, *69*, 302.
19. Zhou, L.; Wang, W.; Zhang, L. *J. Mol. Catal. A: Chem*. **2007**, *268*, 195.
20. Mouider, J. F.; Stickle, W. F.; Soboi, P. E.; Bomben, K. D. *Handbook of X-ray Photoelectron Spectroscopy*; Perkin-Elmer Coporation: USA, 1992; p 90.